Site Specific Optical and Photocatalytic Properties of Bi-Doped NaTaO3

ARTICLE *in* THE JOURNAL OF PHYSICAL CHEMISTRY C · MAY 2011

Impact Factor: 4.77 · DOI: 10.1021/jp2003936

3 AUTHORS, INCLUDING:

Pushkar Kanhere
Techbridge Ventures
20 PUBLICATIONS **389** CITATIONS

SEE PROFILE

THE JOURNAL OF PHYSICAL CHEMISTRY C

ARTICLE

pubs.acs.org/JPCC

Site Specific Optical and Photocatalytic Properties of Bi-Doped $NaTaO_3$

Pushkar D. Kanhere,[†] Jianwei Zheng,[‡] and Zhong Chen*[,†]

[†]School of Materials Science and Engineering, Nanyang Technological University, Block N4.1, 50 Nanyang Avenue, Singapore 639798

[‡]Institute of High Performance Computing, 1 Fusionopolis Way, #16-16 Connexis, Singapore 138632

ABSTRACT: Synthesis, optical properties, and visible light photocatalytic activities of Bi^{3+}-doped $NaTaO_3$ powders have been investigated. The samples were analyzed by X-ray diffraction, X-ray photoelectron spectroscopy, diffused reflectance spectroscopy, and energy dispersive spectroscopy. It is found that the Na/Ta molar ratio of the starting materials affects the site occupancy of Bi at Na or Ta site in the lattice, and thus the optical and photocatalytic properties are significantly altered. Under Na-deficient conditions, Bi predominantly occupied Na site; the sample did not show absorption in the visible region. While under strongly Na-rich conditions, Bi occupancy at Ta site was predominant. These samples showed visible light absorption up to 450 nm. The samples prepared under mildly Na-rich condition, which leads to approximately equal occupancy of Bi at Na and Ta sites, showed visible light absorption up to 550 nm. Correspondingly, the highest photocatalytic activity for methylene blue degradation under visible light was obtained for this condition. The first principles calculation confirmed that band gap narrowing is highest when Bi is substituted at both Na and Ta sites compared with the ones at Na and Ta sites separately. The experimentally observed absorption spectra agree well with that indicated by the electronic structure calculations. The present study shows that the optical property and photocatalytic performance of Bi-doped $NaTaO_3$ can be tuned by Bi occupancy in the lattice. The finding opens up a new venue for designing visible light sensitive ternary compounds for photocatalytical applications.

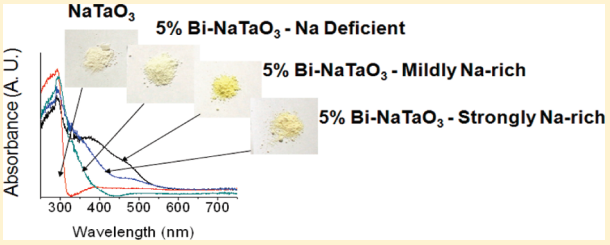

1. INTRODUCTION

In recent years, much attention has been paid to the photocatalytic hydrogen generation which is one of the clean and sustainable ways of harvesting energy. Since the discovery of Honda−Fujishima effect,[1] several classes of materials have been developed for the photocatalytic hydrogen generation.[2−8] Among these materials, tantalum-based oxides such as Ta_2O_5,[9] $MTaO_3$ (M = Na, K, Li, Ag),[10−12] $M_2Ta_2O_7$ (M = Ca, Ba),[13,14] MTa_2O_6 (M = Mg, Ba, Sr),[12,15] and $M_2La_{2/3}Ta_2O_7$ (M = H, K)[16] have shown high activities for hydrogen evolution in pure water. In particular, studies show that $NaTaO_3$ photocatalysts are potential candidates for the efficient water splitting reactions.[17−20] $NaTaO_3$ has favorable band edge potentials and delocalized nature of photoexcited electrons which are the primary reasons for the high efficiency.[18,21,22] The photocatalytic activity of $NaTaO_3$ is further enhanced by doping of alkaline earth ions (Sr, Ba, Ca)[23] and certain lanthanides (e.g., La, Pr, Nd, Sm, Gd, Tb, Dy).[24,25] In a significant development, Kato et al. showed that a maximum of 56% quantum efficiency at 270 nm irradiation can be obtained by 2% La-doped $NaTaO_3$ loaded with (0.5 wt %) NiO ultrafine particles.[26] However, these activities are limited to ultraviolet (UV) region, and the component of UV in the solar spectrum is only about 4%. In order to utilize the solar energy with high conversion efficiency, absorption of wavelengths greater than 420 nm is essential. Doping of foreign elements is one of the most successful ways to alter the band structure of the host material and induce visible light absorption. Therefore, detailed studies on impurity-doped $NaTaO_3$ and their photocatalytic activities are important in order to develop $NaTaO_3$-based photocatalysts for solar energy application.

To date, studies on the visible light active sodium tantalates are limited. Nitrogen-doped $NaTaO_3$ catalyst has been studied for visible light driven photocatalytic degradation of methylene blue[27] as well as gaseous formaldehyde.[28] Codoping of cations such as Cr−La-doped $NaTaO_3$[29,30] and Ir−La-doped $NaTaO_3$[31] has been studied for visible light driven hydrogen evolution. A solid solution photocatalyst ($Na_{1-x}La_xTa_{1-x}Co_xO_3$ for x = 0.0 to x = 0.25) has been developed to tune the band gap to the visible region that showed hydrogen evolution from aqueous methanol solution.[32] These studies suggest that visible light absorption can be achieved by the modification of the band structure via substitutional doping of appropriate cations at Ta site in $NaTaO_3$ lattice. Recently, bismuth-doped $NaTaO_3$ nanoparticles prepared by hydrothermal method have been studied for photocatalytic reactions. Li et al. reported a visible light active solid solution photocatalyst, i.e., $NaTa_{1-x}Bi_xO_3$. Hydrogen evolution over these nanoparticles was reported without any

Received: January 14, 2011
Revised: May 2, 2011
Published: May 20, 2011

cocatalyst loading under visible light radiation.[33] The optical absorption properties of Bi^{3+}-doped $NaTaO_3$ nanoparticles were also studied by Wang et al., where a small change in the band gap of $NaTaO_3$ was seen upon Bi doping.[34] Although there have been reports on Bi-doped $NaTaO_3$, the effect of Bi ion doping on the optical and photocatalytic properties of $NaTaO_3$ is not clear. Orthorhombic $NaTaO_3$ is a close packed structure with Na^+ ions within the corner connected TaO_6 octahedral framework. Ionic radii of Bi^{3+} (1.03 Å), Bi^{5+} (0.76 Å), Na^+ (1.02 Å), and Ta^{5+} (0.64 Å) suggest that replacement of Na^+ by Bi^{3+} and Ta^{5+} by Bi^{5+} is favorable.[35] Thus, substitutional doping of Bi at Na or Ta or both Na and Ta sites is possible under appropriate synthesis conditions. The photocatalytic properties of the materials would significantly change with the substitution site of the dopant in the lattice. To the best of our knowledge, the influence of Bi ions doped at different cation sites, i.e., Na and Ta, in $NaTaO_3$ has not been studied so far. Therefore, detailed investigations on the optical properties and photocatalytic behavior of Bi-doped $NaTaO_3$ powders with different stoichiometry are necessary.

In this study, we report the solid-state synthesis, optical properties, and visible light photocatalytic activities of Bi-doped $NaTaO_3$ powders prepared under strongly Na-rich, mildly Na-rich, and Na-deficient conditions for 5% (moles) bismuth-doped sodium tatalate. It was found that synthesis conditions affect the site occupancy of Bi at Na or Ta site in the lattice, and thus optical and photocatalytic properties have been significantly altered. The samples prepared under mildly Na-rich conditions, which leads to approximately equal occupancy at Na and Ta sites, showed the highest absorption of visible light and the highest rates of methylene blue degradation.

2. EXPERIMENTAL METHODS

2.1. Synthesis. Pristine and Bi-doped $NaTaO_3$ powders were prepared by solid-state reaction. The starting materials, Ta_2O_5 (Aldrich, >99%), Bi_2O_3 (Aldrich, >99%) and Na_2CO_3 (Univar, 99.8%), were mixed in an agate-type mortar, pressed into pellets, and heated at 1173 K for 10 h using a platinum crucible placed in a muffle furnace in ambient atmosphere. Powders were then washed with deionized water and dried in air below 373 K. All the doped samples were prepared with the initial bismuth content of 5% in the starting mixtures. Different synthesis conditions such as strongly Na-rich, mildly Na-rich, and Na-deficient conditions were employed by adjusting the molar ratio of Na_2CO_3 and Ta_2O_5. In all, five samples with fixed (5%) bismuth content but different Na:Ta ratios, viz. 0.950 (Na-deficient), 1.006, 1.010, 1.013 (mildly Na-rich), and 1.050 (strongly Na-rich), hereafter named as B0.950, B1.006, B1.010, B1.013, and B1.050, were synthesized. Because Na has a higher tendency of vaporization loss during sample preparation, the mildly Na-rich sample was aimed at achieving equal occupancy of Bi at Na and Ta site.

2.2. Characterization. The crystal structure of the samples was studied by the X-ray diffraction technique (XRD) (Bruker D8 Advance; Cu Kα = 1.54 Å). The XRD patterns were recorded within 2θ range of 10°−120° with the steps of 0.01° at a scan rate of 1 s per step. The Rietveld refinement of XRD patterns was carried out using Topaz 3.0. In the refinements, profile parameters such as background function (a five-term Chebychev polynomial), zero corrections, scale, and structural parameters such as lattice constants, crystallite size, strain, isothermal parameters, and site occupancies were refined in appropriate order. The location of Bi ions in the lattice was determined from the site occupancy values obtained from the refinements results. A simple crystal structure model is assumed in the refinements where Bi ions are substituted at Na and Ta site in the lattice. To account for the native point defects, occupancy at Na site is countered by vacancy of two Na ions while occupancy of Bi at Ta site is countered by vacancy of one O ion. The ratio of tantalum to bismuth ions in the final powders was estimated by energy dispersive spectroscopy (EDS) analysis carried out using a JOEL6360 scanning electron microscope. The nature of the chemical bonding of bismuth in the doped tantalates was studied by X-ray photoelectron spectroscopy (XPS) (Kratos Axis Ultra, Al Kα source). The analysis of the XPS spectra was carried out using Gaussian functions facilitated in software CASA. The C 1s reference of 284.5 eV was chosen for calibration. The optical properties of the powders were studied by diffused reflectance spectroscopy (DRS) using a UV−vis spectrometer (Perkin-Elmer Lambda 900).

2.3. Photocatalytic Reaction. Photocatalytic behavior of the pristine and Bi-doped powders was studied by photodegradation of methylene blue (MB) in a batch type reactor. In all experiments, 25 mg of catalysts was suspended in 50 mL of 20 ppm MB solution by magnetic stirring and was vertically irradiated using a 300 W lamp (Asahi 320) with internal IR reflector filter. The radiation was restricted to the visible region by a 420 nm cutoff filter. The solution was sampled every hour and centrifuged to filter out the catalyst particles before UV−vis measurement (Shimadzu 2100 spectrometer) to determine the concentration of MB. The blank test was carried out on 20 ppm MB solution without adding any catalyst. In addition, change in the MB concentration under dark conditions was tested for all catalysts as a reference.

3. COMPUTATIONAL METHODS AND MODELS

The electronic structures of pristine and Bi doped $NaTaO_3$ structures were studied by first-principles calculations. All calculations were performed by the projector augmented-wave (PAW) method as implemented in the Vienna *ab initio* Simulation Package (VASP).[36,37] The exchange-correlation functionals was constructed by the Generalized Gradient Approximations (GGA) proposed by Perdew, Burke, and Ernzerhof (PBE).[38] An energy cutoff of 520 eV was employed to describe the electronic wave functions with a plane-wave basis set. The Brillion zone was sampled by Γ point centered Monkhorst−Pack *k*-points mesh of 6 × 6 × 6 for geometry optimization and 10 × 10 × 10 for the calculation of the density of states. The geometry optimization, including atomic positions and lattice parameters were performed on the pristine and doped structures, until the forces on the individual ions were below 0.01 eV/Å and total stress was less than 0.05 GPa. Experimentally reported structure of orthorhombic $NaTaO_3$ (Space Group No. 62 Pbnm)[39] was used as initial structure and the calculated lattice constants are 5.5335, 5.5784, and 7.7869 Å, in good agreement with the experimental data. The substitutional doping of Bi in $NaTaO_3$ was modeled by substituting one Na ion by Bi and one Ta ion by Bi in two separate 2 × 2 × 1 supercells, respectively. Additionally, substitution of Bi ions at both Na and Ta ions was studied. The present substitution accounts for 6.25% of Bi doping in $NaTaO_3$, which is close to the 5% used in the experiments.

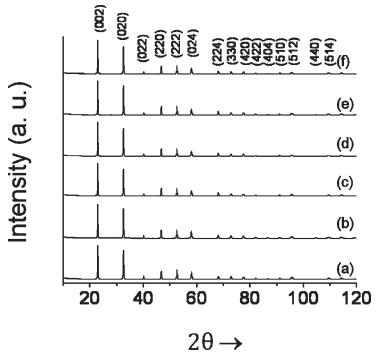

Figure 1. X-ray diffraction patterns of (a) pristine $NaTaO_3$, (b) B0.950, (c) B1.006, (d) B1.010, (e) B1.013, and (f) B1.050.

4. RESULTS AND DISCUSSION

4.1. X-ray Diffraction. X-ray diffraction (XRD) patterns of the samples, viz. pristine $NaTaO_3$, B0.950, B1.006, B1.010, B1.013, and B1.050, are shown in Figure 1. All the samples show the presence of monophase and belong to the same space group as of pristine $NaTaO_3$ (space group no. 62 Pbnm). The Rietveld refined lattice parameters and unit cell volumes (a = 5.4834, Å b = 5.5228 Å, c = 7.7933 Å; V = 236.012 Å^3) of the pristine $NaTaO_3$ are in good agreement with the values reported in the literature.[39,40] Impurity-free XRD patterns indicate that Bi has been fully accommodated in the lattice sites. Figure 2 shows the unit cell volume of the samples obtained from Rietveld refinements. Each data point is an average of five measurements and is plotted along with the standard deviation. In order to study the effect of synthesis conditions on the unit cell volume, two additional samples with Na/Ta ratio 0.98 and 1.02 were synthesized and analyzed (Figure 2). All the doped samples show increase in the unit cell volume compared to the pristine $NaTaO_3$. Further, it is observed that the changes in the unit cell volume are sensitive to the doping condition. A maximum increase in the unit cell volume was seen for the samples prepared under Na-deficient conditions, followed by those prepared under strongly Na-rich and mildly Na-rich conditions. The unit cell volume change is a compounded effect of impurity accommodation and presence of native point defects. Therefore, it is clear that changes in the synthesis conditions are responsible for observed unit cell volume change. The charge neutrality equations of Bi accommodation at Na and Ta sites in $NaTaO_3$ lattice can be summarized as follows:

$$(Na^+) = (Bi^{3+}) - 2(Na^+) \quad \text{(I)}$$

$$(Na^+) = (Bi^{3+}) - (Ta^{5+}) + (Na^+) - (O^{2-}) \quad \text{(II)}$$

$$(Na^+) = (Bi^{3+}) - (Ta^{5+}) + 3(Na^+) \quad \text{(III)}$$

$$(Ta^{5+}) = (Bi^{3+}) - (O^{2-}) \quad \text{(IV)}$$

$$(Ta^{5+}) = (Bi^{5+}) \quad \text{(V)}$$

$$(Na^+) + (Ta^{5+}) = 2(Bi^{3+}) \quad \text{(VI)}$$

The sample B0.950 is prepared under Na-deficient conditions, where the numbers of moles of Na and Bi are equal to the number of moles of Ta ions ($M_{Na} + M_{Bi} = M_{Ta}$). Thus, under this condition the occupancy of Bi at Na site together with cation vacancies is favorable according to eqs I−III. Similarly, sample B1.050 was prepared under strongly Na-rich conditions, where $M_{Na} > M_{Ta} + M_{Bi}$. Thus, the occupancy of Bi at Ta site with oxygen vacancy formation is favorable (eq IV). Alternatively substitution of Bi^{5+} at Ta^{5+} may also be possible as suggested by eq V. The initial stoichiometry of the samples prepared under mildly Na-rich conditions implies that Bi^{3+} occupancy at both Na and Ta site is likely favorable. In this case, the ionic charge neutrality is maintained and thus the concentration of the native defects is likely to be minimal (eq VI). It is noted that Bi occupancy at both sites maintains ionic charge balance and causes minimum distortion in the lattice. Thus, under perfect stoichiometric conditions, occupancy at both sites would be energetically favorable. Table 1 shows results of the Rietveld refinements performed on the X-ray diffraction patterns of pristine and doped samples. A systematic trend in the site of occupancies of Bi ions at Na and Ta sites is observed along with the changes in the synthesis conditions. As the synthesis conditions become Na-rich, occupancy at Na site is decreased and that at Ta site is increased. These values show that under Na-deficient conditions Bi predominantly occupies Na site while under strongly Na-rich conditions Bi ions predominantly occupy Ta site. Further, when the synthesis conditions are maintained in between the two, i.e., mildly Na-rich, Bi ions tends to occupy both Na and Ta sites approximately in equal proportion. Earlier studies have shown that dopant site in the crystal structure of simple perovskites can be controlled by adjusting the stoichiometry of the initial reactants.[41,42] The behavior of the unit cell volume thus arises from different site occupancies of Bi ions in $NaTaO_3$ lattice, and respective native point defects are produced.

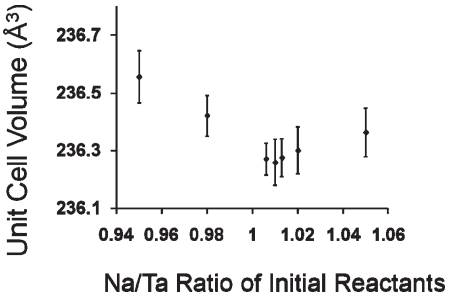

Figure 2. Variation in unit cell volumes of Bi-doped $NaTaO_3$ samples prepared under different synthesis conditions.

4.2. XPS Analysis. In order to investigate the formal oxidation state and chemical environment of the Bi ions in the doped samples, X-ray photoemission (XPS) spectroscopy analysis was carried out. XPS spectra of Bi 4f, O 1s, and Ta 4f were analyzed in the pristine and doped samples. Figure 3 shows Bi 4f spectra of the samples B0.950, B1.006, B1.010, B1.013, B1.050, and pristine Bi_2O_3. The peaks in XPS spectra at around 158.35 and 163.65 eV are assigned to bismuth $4f_{7/2}$ and $4f_{5/2}$ in the Bi^{3+} oxidation state. There were no obvious higher energy components corresponding to Bi^{5+}. Earlier studies on bismuth compounds have suggested that Bi^{5+} peak appears around 2 eV higher than that of Bi^{3+}.[43] Thus, the possibility of Bi^{5+} is eliminated in the current study. The binding energies of Bi 4f follow a trend, i.e., Na-deficient > strongly Na-rich > mildly Na-rich > Bi_2O_3 (Table 2). Pristine Bi_2O_3 shows single component for Bi $4f_{7/2}$ and $4f_{5/2}$ peaks. However, the peaks in all the doped samples show two

Table 1. Results of Rietveld Refinements of X-ray Diffraction Patterns of Pristine and Bi-Doped $NaTaO_3$ Powders

sample	$NaTaO_3$	B0.950	B1.006	B1.050
cell volume (Å^3)	236.0822 (54)	236.4231 (81)	236.2159 (65)	236.2661 (73)
a (Å)	5.486354 (75)	5.49524 (11)	5.488963 (90)	5.491133 (99)
b (Å)	5.521300 (70)	5.51793 (10)	5.521277 (84)	5.520547 (91)
c (Å)	7.79360 (10)	7.79700 (16)	7.79434 (13)	7.79395 (15)
crystallite size (nm)	180 (14)	126.7 (67)	166.1 (13)	146.7 (98)
strain (%)	0.1562 (20)	0.2374 (27)	0.1893 (24)	0.2154 (27)
occupancy Bi (Na)		0.0277 (11)	0.0183 (15)	0.0136 (14)
occupancy Bi (Ta)		0.0009 (81)	0.0307 (10)	0.0363 (94)
B_{Na} (Å^2)	1.2050 (60)	1.5260 (67)	1.4760 (94)	1.3550 (86)
B_{Ta} (Å^2)	0.4318 (95)	0.3987 (73)	0.2659 (94)	0.3869 (87)
R_{wp} (%)	6.7620	5.0970	6.6490	6.0550
R_{Bragg} (%)	1.984	1.117	1.703	1.500

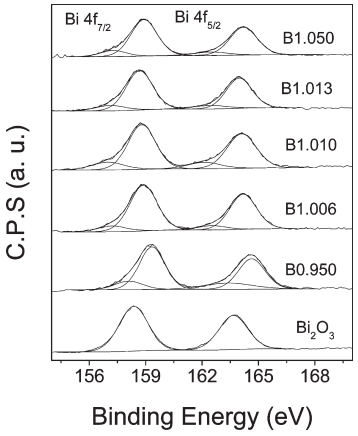

Figure 3. XPS spectra of Bi $4f_{7/2}$ and Bi $4f_{5/2}$ of Bi_2O_3 and Bi-doped $NaTaO_3$.

Table 2. Carbon Corrected Binding Energies (eV) of Bi 4f Components of Pristine Bi_2O_3 and Bi-Doped $NaTaO_3$ Samples

	BE (eV)			
sample	Bi $4f_{7/2}$		Bi $4f_{5/2}$	
Bi_2O_3	158.35		163.65	
B0.950	159.33	158.11	164.63	163.41
B1.006	158.91	157.20	164.18	162.53
B1.010	158.78	156.84	164.11	162.12
B1.013	158.71	157.29	163.97	162.44
B1.050	158.91	157.14	164.2	162.51

components in binding energy peaks, indicating the presence of more than one chemical environment. As mentioned earlier, occupancy of Bi ions at both Na and Ta sites is energetically favorable. However, under Na-rich or Na-deficient conditions the occupancy at Ta and Na site is prominent, respectively. Thus, the differences in the binding energies are attributed to differences in the chemical environment, i.e., different sites in the $NaTaO_3$ lattice. Figure 4 shows O 1s spectra in the pristine $NaTaO_3$ and Bi-doped $NaTaO_3$ samples. The binding energy values of O 1s in all the doped structure are greater than those in

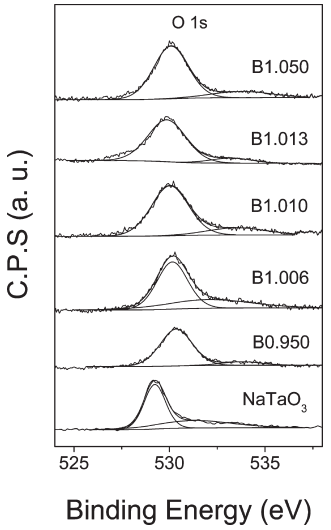

Figure 4. XPS spectra of O 1s of pristine and Bi-doped $NaTaO_3$.

pristine $NaTaO_3$ (Table 3). Similar to the Bi 4f peaks, the chemical shifts in the binding energy of O 1s spectra may be attributed to the replacement of Na−O and Ta−O bonds by Bi−O bonds in the doped samples. Although the local structure, i.e., location of Bi ions in the lattice cannot be conclusively studied by using the XPS technique, the trends in the binding energy values suggest that different chemical environments are present under different synthesis conditions.

4.3. Energy Dispersive Spectroscopy. The amount of bismuth in the final powders was analyzed by using the energy dispersive spectroscopy (EDS) technique by recoding the cation ratios of tantalum to bismuth in all the samples. EDS analysis of the doped samples show presence of Na, Ta, Bi, and O while no bismuth was found in pristine $NaTaO_3$ sample. EDS analysis reveals that the bismuth content in the final powders ranges between 4% and 5% with respect to tantalum content (Table 4, Ta:Bi ratio ranging between 20 and 24). The values presented in the Table 4 are the average values of reading taken over four different areas of the sample. In all the starting mixtures the content of bismuth was 5% with respect to tantalum content, i.e., Ta/Bi ions ratio was set to 20. The little loss of bismuth is attributed to evaporation at high temperatures. The present analysis shows that doped samples have nearly equal bismuth

Table 3. Carbon Corrected Binding Energies (eV) of O 1s Components of Pristine and Bi-Doped $NaTaO_3$

	BE (eV)	
sample	O 1s	O 1s
$NaTaO_3$	529.23	531.31
B0.950	530.38	533.81
B1.006	530.15	532.05
B1.010	530.04	533.46
B1.013	529.89	531.92
B1.050	530.08	533.69

Table 4. Ratios of Ta/Bi Obtained from Energy Dispersive Spectroscopy Analysis of Bi-Doped $NaTaO_3$ Samples

sample	ratio (Ta:Bi)	sample	ratio (Ta:Bi)
$NaTaO_3$		B1.010	24.2621
B0.950	20.9832	B1.013	21.8548
B1.006	21.5213	B1.050	24.0786

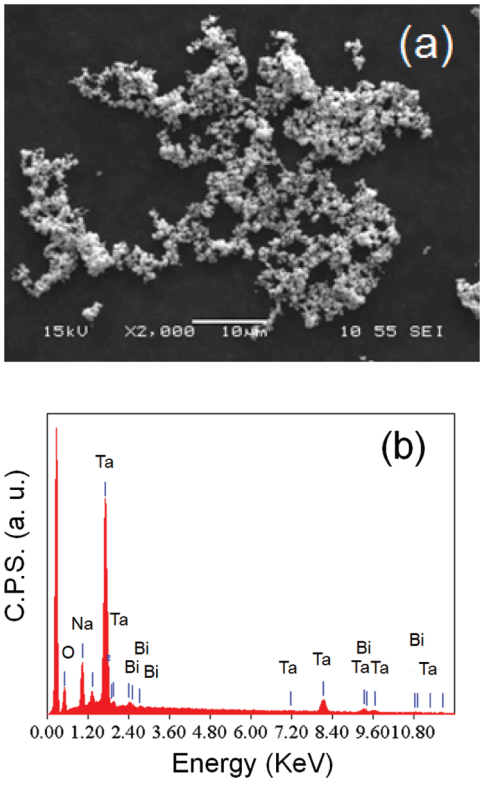

Figure 5. (a) Secondary electron image and (b) energy dispersive spectra of sample B1.050.

content, and thus the changes in the optical and photocatalytic properties are not due to variation in Bi doping. SEM images of all the samples show micrometer sized particles with large particle size variation. Figure 5 shows a representative secondary electron image and EDS spectra of B1.050.

4.4. Optical Properties. The optical absorption spectra of the samples B0.950, B1.006, B1.010, B1.013, and B1.050 are

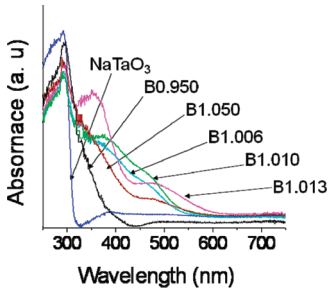

Figure 6. Diffused reflectance spectra of pristine and Bi-doped $NaTaO_3$ samples.

compared with that of pristine $NaTaO_3$ in Figure 6. The band gap of the pristine $NaTaO_3$ is found to be 4.01 eV. The absorption spectra of all of the Bi-doped samples show extension toward longer wavelength. The absorption spectra of B0.950 sample do not show visible light absorption; thus, the band gap value is in the UV region. The samples prepared under mildly Na-rich conditions B1.006, B1.010, and B1.013 show intense visible light absorption extending up to 550 nm. Lastly, the sample prepared under strongly Na-rich conditions, i.e., B1.050, shows little extension in the visible region as compared to the samples prepared under mildly Na-rich conditions. Thus, samples prepared under mildly Na-rich conditions show maximum visible light absorption, compared to those prepared under Na-deficient and strongly Na-rich conditions. The above results indicate that extent of the visible light absorption is dependent on the initial stoichiometry of the starting materials. As indicated by XRD analysis, the initial molar ratios affect the substitution site of the Bi in the lattice; thus, the band gap values are the functions of the substitution site of Bi in $NaTaO_3$. The origin of the differences in the optical spectra can be understood on the basis of band structure calculations, which will be discussed in the following section.

4.5. Electronic Structure and Density of States Analysis (DOS) of $NaTa_{1-x}Bi_xO_3$, $Na_{1-x}Bi_xTaO_3$, and $Na_{1-x}Bi_xTa_{1-x}Bi_xO_3$. Analysis of the density of states (DOS) of pristine $NaTaO_3$ shows that top of the valence band (VB) is predominantly composed of O 2p while the conduction band (CB) mainly consists of Ta 5d orbitals. Thus, upon the photoexcitation the transition of electrons from O 2p to empty Ta 5d occurs. The band gap value of this structure is found to be 2.637 eV, which is in agreement with the reported literature.[44,45] Though GGA underestimates the band gap for semiconductors, the comparison of the relative results cancels out the errors and thus the change in band gap value due to doping is taken into consideration. The electronic structure of the doped photocatalysts such as TiO_2 and $SrTiO_3$ has been widely studied by DFT.[46,47] The comparison of DOS of pristine and Bi-doped $NaTaO_3$ structures reveals that new energy states in between the band gap occur on Bi doping. These midgap states are responsible for a band gap reduction of 0.87, 0.15, and 1.5 eV for the substitution of Bi at Ta site, Bi at Na site, and Bi at both Na and Ta sites, respectively (Figure 7). The site projected partial DOS in Figure 8 shows that the substitution of Bi at Ta site induces energy states below the conduction band minimum (CBM). These states are mainly composed of Bi 6s + O 2p + Ta 5d orbitals, indicating that the transition from O 2p to Bi 6s occurs during photoexcitation. On the other hand, the substitution of Bi at Na site creates new states above the valence band maximum (VBM). They appear as a

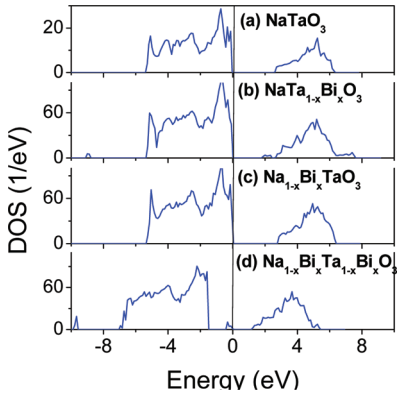

Figure 7. Total density of states (DOS) of (a) pristine $NaTaO_3$, (b) $NaTa_{1-x}Bi_xO_3$, (c) $Na_{1-x}Bi_xTaO_3$, and (d) $Na_{1-x}Bi_xTa_{1-x}Bi_xO_3$ ($x = 0.0625$).

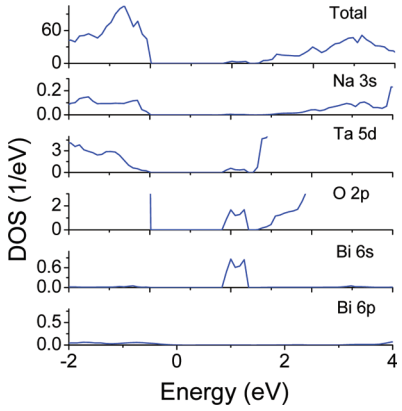

Figure 8. Electronic partial density of states (PDOS) of $NaTa_{1-x}Bi_xO_3$ ($x = 0.0625$).

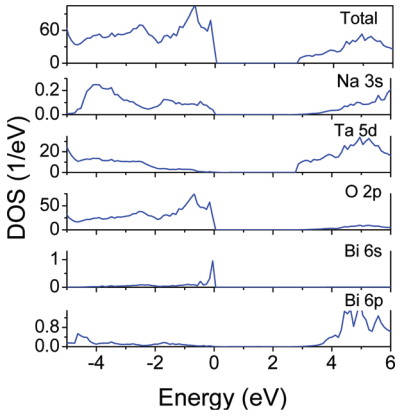

Figure 9. Electronic partial density of states (PDOS) of $Na_{1-x}Bi_xTaO_3$ ($x = 0.0625$).

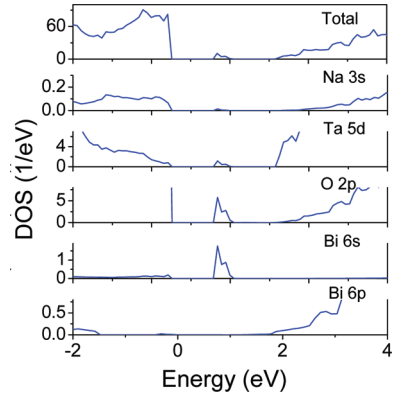

Figure 10. Electronic partial density of states (PDOS) of $Na_{1-x}Bi_x$-$Ta_{1-x}Bi_xO_3$ ($x = 0.0625$).

shoulder to the VB. These states are formed by Bi 6s + O 2p orbitals (Figure 9). When Bi is substituted at both Na and Ta sites, extra states appear midway in the band gap (Figure 10). These states are located at 1.05 eV above the VB and consist of Bi 6s + O 2p + Ta 5d orbitals. For Bi substitution at Na site and at both Na and Ta sites, DOS analysis suggests that electronic transition from filled Bi 6s to empty Ta 5d takes place. In all the cases, it is clear that the band gap narrowing is caused by the newly formed energy states derived from Bi 6s orbitals, indicating that bismuth accommodation in the lattice is the cause of band gap reduction. Finally, we compare the optical properties of the samples with electronic structure calculation results. The structural characterization of the samples shows that under Na-deficient, mildly Na-rich, and strongly Na-rich conditions the occupancy of Bi ions at Na site, both Na and Ta site, and Ta site is predominant, respectively. The sample B0.950 (Na-deficient) shows negligible absorption in the visible region while sample B1.050 (strongly Na-rich) shows absorption up to 450 nm. The samples B1.006, B1.010, and B1.013 (mildly Na-rich), however, show the highest visible light absorption extending up to 550 nm. The decrease in the band gap values predicated by DFT calculations (0.15 eV for Bi at Na site, 1.5 eV for Bi at both Na and site, 0.87 eV for Bi at Ta site) follows the same trend as observed in the optical absorption spectra of the samples prepared under Na-deficient, mildly Na-rich, and strongly Na-rich conditions, respectively. Thus, the optical properties indicated by the band structure calculations are in good agreement with the experimentally observed absorption spectra. Although our DFT calculations do not account for point defects, the calculations help to understand the role of Bi ions in the valence electronic structure of $NaTaO_3$ lattice. The concentration and nature of these point defects are not known experimentally; therefore, the appropriate model for DFT simulations is unknown. Earlier study has shown that native point defects have no effect on the band gap of $NaTaO_3$.[45]

4.6. Photocatalytic Activity (MB Degradation). Finally, we compare the photocatalytic activities of Bi-doped $NaTaO_3$ prepared under different conditions, under visible light (>420 nm). Figure 11 shows UV−vis absorption spectra of MB solution with B1.006 sample, exposed to visible light. The absorption peak corresponding to MB is systematically decreased with time, indicating photocatalytic degradation occurred over B1.006 sample. Under dark conditions, no significant change in the concentration of MB solution was observed for any of the catalysts. Figure 12 compares degradation rates of MB over different catalyst under visible radiation. There was about 30% decrease of initial concentration MB without any catalyst (blank test). It was due to photolysis, which has been reported before in a similar case.[48] The samples prepared under mildly Na-rich conditions (B1.006, B1.010, and B1.013) show the highest degradation rates among all. (The samples B1.010 and B1.013

dx.doi.org/10.1021/jp2003936 |J. Phys. Chem. C 2011, 115, 11846–11853

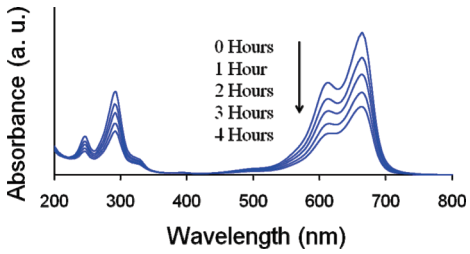

Figure 11. Absorption spectra of methylene blue solution with B1.006 catalyst, irradiated under visible light (>420 nm).

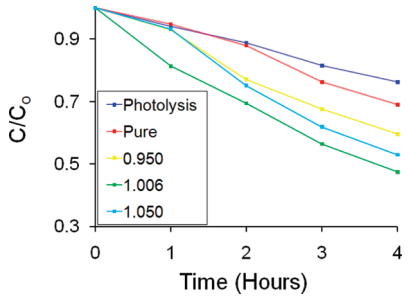

Figure 12. C/C_0 curves of methylene blue degradation over pristine and Bi-doped $NaTaO_3$ samples under visible radiation (>420 nm).

also showed similar degradation rates as that of sample B1.006.) The degradation rate of pristine $NaTaO_3$ is similar to that of photolysis of MB. The photocatalytic activities show a clear gradation between the performances as follows: mildly Na-rich > strongly Na-rich > Na-deficient. This behavior of the samples is consistent with the optical absorption properties. The samples prepared under mildly Na-rich conditions absorb higher amount of visible light and longer wavelength than other samples. Lower amount of absorption of visible light is the primary reason for lower activities of B0.950 and B1.050 samples. It is further noted that, under strongly Na-rich and Na-deficient conditions, native point defects are present as expressed in eqs I–IV. However, under mildly Na-rich conditions, Bi^{3+} ions have approximately equal occupancies, and thus the ionic charge balance in the lattice is maintained which leads to minimization of the points defects produced on bismuth doping. Thus, reduced defects may be an additional contributing factor for the higher activity in mildly Na-rich samples.

5. CONCLUSIONS

Bi^{3+}-doped $NaTaO_3$ powders are synthesized under different stoichiometric conditions by the conventional solid-state route. The optical and photocatalytic properties of doped powders are investigated, and their correlation with the location of bismuth in the lattice is established using experimental techniques as well as the first principles electronic structure calculations.

Our investigations reveal that controlling the stoichiometry of the initial reactants, the occupancy of Bi at Na and Ta site in the lattice can be controlled and thus the optical properties can be successfully altered. Under Na-deficient conditions and strongly Na-rich conditions, Bi predominantly occupies Na and Ta site in the lattice, respectively. Bi doping at Na site of $NaTaO_3$ is not useful to induce visible light absorption while Bi doping at Ta site induces visible light absorption limited to 450 nm. Under mildly Na-rich conditions, Bi ions occupy both Na and Ta site in approximately equal proportion, which gives rise to the highest visible light absorption up to 550 nm. Consequently, these samples also show the highest rates of MB degradation under visible light, >420 nm. The electronic structure calculations reveal that substitutional doping of Bi at Ta site, Na site, and both Na and Ta site induces midgap states consisting of Bi 6s orbitals and the effective band gap is narrowed by 0.8, 0.15, and 1.50 eV, respectively. The present results indicate that selective Bi occupancy at different cation lattice sites can be a useful way to adjust the visible light photocatalytic properties of doped $NaTaO_3$ semiconductor materials.

AUTHOR INFORMATION

Corresponding Author

*E-mail: aszchen@ntu.edu.sg. Tel: +65-6790-4256. Fax: +65-6790 9081.

ACKNOWLEDGMENT

Financial support from MOE Singapore (Grant RG 112/05) and A*Star Singapore (Grant SERC 0521010016) is gratefully acknowledged. We are grateful to Dr. Martin K. Schreyer in ICES for the numerous technical discussions on crystal structures.

REFERENCES

(1) Fujishima, A.; Honda, K. *Nature* **1972**, *238*, 37–38.
(2) Kudo, A.; Miseki, Y. *Chem. Soc. Rev.* **2009**, *38*, 253–278.
(3) Inoue, Y. *Energy Environ. Sci.* **2009**, *2*, 364–386.
(4) Osterloh, F. E. *Chem. Mater.* **2008**, *20*, 35–54.
(5) Kudo, A. *Int. J. Hydrogen Energy* **2007**, *32*, 2673–2678.
(6) Kudo, A. *Catal. Surv. Asia* **2003**, *7*, 31–38.
(7) Kudo, A. *Int. J. Hydrogen Energy* **2006**, *31*, 197–202.
(8) Kitano, M.; Hara, M. *J. Mater. Chem.* **2010**, *20*, 627–641.
(9) Takahara, Y.; Kondo, J. N.; Takata, T.; Lu, D.; Domen, K. *Chem. Mater.* **2001**, *13* (4), 1194–1199.
(10) Kato, H.; Kudo, A. *J. Phys. Chem. B* **2001**, *105*, 4285–4292.
(11) Kato, H.; Kobayashi, H.; Kudo, A. *J. Phys. Chem. B* **2002**, *106*, 12441–12447.
(12) Kato, H.; Kudo, A. *Chem. Phys. Lett.* **1998**, *295*, 487–492.
(13) Kudo, A.; Kato, H.; Nakagawa, S. *J. Phys. Chem. B* **2000**, *104*, 571–575.
(14) Ikeda, S.; Fubuki, M.; Takahara, Y. K.; Matsumura, M. *Appl. Catal., A* **2006**, *300*, 186–190.
(15) Kato, H.; Kudo, A. *Chem. Lett.* **1999**, *11*, 1207–1208.
(16) Shimizu, K. I.; Itoh, S.; Hatamachi, T.; Kodama, T.; Sato, M.; Toda, K. *Chem. Mater.* **2005**, *17*, 5161–5166.
(17) Kato, H.; Kudo, A. *Catal. Lett.* **1999**, *58*, 153–155.
(18) Kato, H.; Kudo, A. *J. Phys. Chem. B* **2001**, *105*, 4285–4292.
(19) Lin, W. H.; Hu, C. C.; Teng, H. J. *Appl. Phys. Lett.* **2006**, *89*, 211904.
(20) Lee, Y. W.; Takata, T.; Hara, T.; Yoshimura, M.; M. Domen, K. *Bull. Chem. Soc. Jpn.* **2007**, *80*, 423–428.
(21) Hu, C. C.; Tsai, C. C.; Teng, H. *J. Am. Ceram. Soc.* **2009**, *92*, 460–466.
(22) Yamakata, A. I.; T., A.; Kato, H.; Kudo, A.; Onishi, H. *J. Phys. Chem. B* **2003**, *107*, 14383–14387.
(23) Iwase, A.; Kato, H.; Kudo, A. *ChemSusChem* **2009**, *2*, 873–877.
(24) Yan, S. C.; Wang, Z. Q.; Li, Z. S.; Zou, Z. G. *Solid State Ionics* **2009**, *180*, 1539–1542.
(25) Kudo, A.; Kato, H. *Chem. Phys. Lett.* **2000**, *331*, 373–377.
(26) Kato, H.; Asakura, K.; Kudo, A. *J. Am. Chem. Soc.* **2003**, *125*, 3082–3089.

(27) Liu, D. R.; Wei, C. D.; Xue, B.; Zhang, X. G.; Jiang, Y. S. *J. Hazard. Mater.* **2010**, *182*, 50–54.
(28) Fu, H. Z. S.; Zhang, L.; Zhu, Y. *Mater. Res. Bull.* **2008**, *43*, 864–872.
(29) Yi, Z. G.; Ye, J. H. *J. Appl. Phys.* **2009**, *106*, 074910.
(30) Yang, M.; Huang, X.; Yan, S.; Li, Z.; Yu, T.; Zou, Z. *Mater. Chem. Phys.* **2010**, *121*, 506–510.
(31) Iwase, A.; Saito, K.; Kudo, A. *Bull. Chem. Soc. Jpn.* **2009**, *82*, 514–518.
(32) Yi, Z. G.; Ye, J. H. *Appl. Phys. Lett.* **2007**, *91*, 254108.
(33) Li, Z. W.; Liu, Y.; Chen, J.; Li, G.; Y. Zhou, C. *Int. J. Hydrogen Energy* **2009**, *34*, 147–152.
(34) Wang, X.; Bai1, H.; Meng, Y.; Zhao, Y.; Tang, C.; Gao, Y. *J. Nanosci. Nanotechnol.* **2010**, *10*, 1788–1793.
(35) Shannon, R. D. *Acta Crystallogr., Sect. A: Found. Crystallogr.* **1976**, 751.
(36) Kresse, G.; Joubert, D. *Phys. Rev. B* **1999**, *59*, 1758–1775.
(37) Kresse, G.; Furthmüller, J. *Phys. Rev. B* **1996**, *54*, 11169–11186.
(38) Perdew, J. P.; Burke, K.; Ernzerhof, M. *Phys. Rev. Lett.* **1996**, *77*, 3865–3868.
(39) Ahtee, M.; Darlington, C. N. W. *Acta Crystallogr., Sect. B: Struct. Sci.* **1980**, *36*, 1007–1014.
(40) Kennedy, B. J.; Prodjosantoso, A. K.; Howard, C. J. *J. Phys.: Condens. Matter* **1999**, *11*, 6319–6327.
(41) Wang, D.; Ye, J.; Kako, T.; Kimura, T. *J. Phys. Chem. B* **2006**, *110*, 15824–15830.
(42) Lin, M. H.; Lu, H. Y. *Mater. Sci. Eng., A* **2002**, *335*, 101–108.
(43) Fujimoto, Y. *J. Am. Ceram. Soc.* **2010**, *93*, 581–589.
(44) Li, Z. H.; Chen, G.; Liu, J. W. *Solid State Commun.* **2007**, *143*, 295–299.
(45) Choi, M.; Oba, F.; Tanal, I. *Phys. Rev. B* **2008**, *78*, 014115.
(46) Yang, K.; Dai, Y.; Huang, B.; Whangbo, M. H. *Chem. Mater.* **2008**, *20*, 6528–6534.
(47) Wei, W.; Ying, D.; Meng, G.; Lin, Y.; Baibiao, H. *J. Phys. Chem. C* **2009**, *113*, 15046–15050.
(48) Zhao, Y.; Qiu, X.; Burda, C. *Chem. Mater.* **2008**, *20*, 2629–2636.